

Application of Bessel Beam for Doppler Velocity Estimation

Jian-Yu Lu, *Member, IEEE*, Xiao-Liang Xu, *Member, IEEE*, Hehong Zou, and James F. Greenleaf, *Fellow, IEEE*

Abstract— Limited-diffraction beams have a large depth of field and could be applied to medical imaging, tissue characterization, and nondestructive evaluation of materials. This paper reports the application of limited-diffraction beams, specifically, the Bessel beam, to Doppler velocity estimation. The Bessel beam has the advantage that velocity estimation is less subject to the depth of moving objects and the Doppler spectrum has distinct shoulders that increase the accuracy of velocity (both magnitude and Doppler angle) estimation in noisy environments. The shoulders of the Doppler spectrum might also help in solving the inverse problem, e.g., estimation of the velocity distribution in vessels.

I. INTRODUCTION

THE Doppler effect was discovered by the Austrian physicist, Christian Doppler in 1843 [1]. It has been applied to electromagnetic waves [2] and medical ultrasound such as the estimation of blood flow with backscattered continuous wave (CW) [3], pulsed wave (PW) [4], imaging of blood vessels [5], and color flow mapping [6]. Recently, Doppler spectral broadening due to the beam geometry has been analyzed [7] and applied to the estimation of the flow velocity component that is perpendicular to the beam axis [8]–[13].

In previous studies, beams designed to use the Doppler effect or spectrum broadening were either plane waves or conventional focused beams. The plane wave can not define a lateral position and thus has low resolution in imaging. Conventional focused beams can produce high resolution at their focuses but have a short depth of field and thus the shape of their Doppler spectra may change with depth.

The first beam that can focus over a large depth was found in electromagnetics by Brittingham [14] and was called focus wave mode (FWM). The FWM was further studied by Ziolkowski et al. [15], [16]. Limited-diffraction beams, which were originally called nondiffracting beams, were first discovered by Durnin in 1987 [17]. These beams have a large depth of field [18]–[23] and might have applications in medical ultrasonic imaging [24]–[26], tissue characterization [27], [28], and nondestructive evaluation of materials [29], and other physics related areas such as electromagnetics [30], [31] and optics [32]–[40]. Because of the large depth of field of the limited diffraction beams, theoretically, flow estimation with these beams should be depth-independent.

Manuscript received June 27, 1994; revised November 15, 1994. This work was supported in part by grants CA 43920 and CA 54212 from the National Institutes of Health.

The authors are with the Biodynamics Research Unit, Department of Physiology and Biophysics, Mayo Clinic and Foundation, Rochester, MN 55905 USA.

IEEE Log Number 9410105.

With the Doppler effect, one can only estimate the velocity component that is parallel to the beam axis. Doppler spectrum broadening which is caused by amplitude modulation of the received signal, is related to the velocity component that is perpendicular to the beam axis. From these two components, the magnitude of velocity and its angle with the beam axis can be calculated. It has been shown that the maximum and minimum frequency points of the Doppler spectrum of a conventional focused piston beam are independent of the axial distance of a moving object [11]. However, the shape of the Doppler spectrum may change with distance. For example, the shape of the Doppler spectrum of a focused piston beam is triangular only near the focus [9]. Therefore, in a noisy environment where the maximum and the minimum frequency points of the spectrum are difficult to measure directly, it is difficult to obtain a consistent estimation of the bandwidth of the spectrum and thus the velocity component that is perpendicular to the beam axis over distance. Furthermore, for a focused Gaussian beam, theoretically, there are no finite maximum and minimum frequency points in the Doppler spectrum at the focal plane (the Fourier transform of a Gaussian function is Gaussian). In this case, the estimation of bandwidth and thus the transverse velocity component of a moving object depends entirely on the shape of the spectrum.

In this paper, we apply limited-diffraction beams, specifically, the Bessel beam [17], to velocity estimation using the Doppler effect. Because the Bessel beam has a large depth of field, both the shape and the maximum and minimum frequency points of its Doppler spectrum are less dependent on the distance of moving objects. In addition, the Doppler spectrum of the Bessel beam for an object moving at a constant velocity has distinct shoulders representing the lower and upper boundaries of the spectrum that are related to both the angle and the magnitude of the velocity of the object. Because of the shoulders, the velocity vector estimation may be more accurate and less subject to noise. These features of the Bessel beam are derived theoretically, demonstrated with computer simulation, and verified with experiment.

In the following, we first derive the Doppler spectra of a Bessel beam for various moving objects. Then we demonstrate the theoretical results with computer simulation. Experimental results are then reported. Finally, we give a brief discussion and conclusion.

II. THEORY

We first give the formula of a limited-diffraction beam, specifically the Bessel beam, and then derive the Doppler spectra for various moving objects.

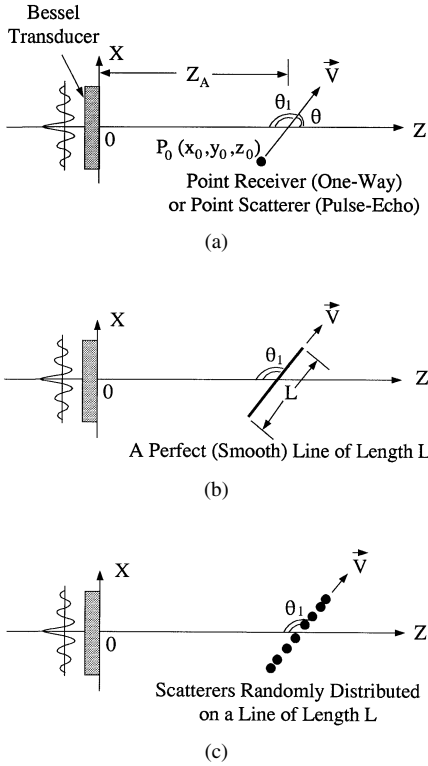


Fig. 1. Velocity estimation with a Bessel beam. The axis of the Bessel beam is at $x = 0$ and $y = 0$. z_A is the distance between the intersection of the projection of the velocity, \vec{v} , on the plane $y = 0$ and the surface of the Bessel transducer. Because the Bessel beam is axially symmetric, we can always assume that the velocity, \vec{v} , is in parallel with the plane, $y = 0$. P_0 represents a point receiver or a point scatterer located at (x_0, y_0, z_0) (Panel (a)). $L = 50$ mm is either the length of a smooth line segment (Panel (b)) or that of a line of random scatterers (Panel (c)) moving at the velocity, \vec{v} . L is centered at $(0, 0, z_A)$ when time $t = 0$. θ and θ_1 are complementary about π . θ_1 is used to indicate the Doppler angle for all other figures that show a positive frequency shift when $\theta_1 < \pi/2$.

A. Bessel Beam

One of the limited-diffraction beams, called the Bessel beam, is given by [17]

$$\Phi_{J_0}(\vec{r}, t) = A J_0(\alpha r) e^{i(\beta z - \omega t)}, \quad (1)$$

where A is a complex constant that relates to the gain and initial phase of a system (without losing generality, we assume $A \equiv 1$), $\Phi_{J_0}(\cdot)$ represents the pressure or velocity potential of an acoustic wave (or scalar components of an electromagnetic wave), $J_0(\cdot)$ is the zeroth-order Bessel function of the first kind, $\vec{r} = (r, \phi, z)$ represents a point in space, $r = \sqrt{x^2 + y^2}$, $\phi = \tan^{-1}(y/x)$ is the azimuthal angle in a transverse plane of the beam, z is the axial distance, t is time, α denotes a scaling factor that determines the beam width, $\beta = \sqrt{k^2 - \alpha^2} > 0$, in which $k = \omega/c$ is the wave number, $\omega = 2\pi f$ is the angular frequency and f is the frequency, and c is the speed of sound in the medium.

If the Bessel beam is approximately produced with a finite aperture, it has a finite depth of field

$$BZ_{max} = a \sqrt{(k/\alpha)^2 - 1}, \quad (2)$$

which is much larger than that of a conventional beam (where a is the radius of a circular aperture).

B. Doppler Spectrum of Signal Measured by a Moving Receiver

We first describe the one-way Doppler spectrum in which a point receiver moves in a Bessel beam. This simple case will demonstrate the fundamentals to be used in the theoretical analysis of the two-way (pulse-echo or backscattered) Doppler spectrum. Assume that a point receiver is located in the plane, $y = y_0$, moving at a velocity, v , across the axis of a Bessel beam at an angle, θ (Fig. 1(a)). The motion of the receiver can be described with

$$\begin{cases} x = x_0 + vt \sin \theta \\ y = y_0 \\ z = z_0 + vt \cos \theta \end{cases}, \quad (3)$$

where the coordinates, (x_0, y_0, z_0) , represent the original position of the receiver (at $t = 0$). If we ignore the secondary Doppler effect (the Doppler effect caused by the change of f or β) in (1), the signal received is given by

$$g(\vec{r}_0, t) = J_0 \left(\alpha \sqrt{(x_0 + vt \sin \theta)^2 + y_0^2} \right) \cdot e^{i(\beta_0(z_0 + vt \cos \theta) - \omega_0 t)}, \quad (4)$$

where $\omega_0 = 2\pi f_0$, f_0 is the transmitted frequency, $\beta_0 = \sqrt{k_0^2 - \alpha^2}$, and $k_0 = \omega_0/c$.

Eq. (4) can be rewritten as

$$g(\vec{r}_0, t) = J_0 \left(\alpha v \sin \theta \sqrt{\left(t - \frac{-x_0}{v \sin \theta} \right)^2 + \left(\frac{y_0}{v \sin \theta} \right)^2} \right) \cdot e^{i(\beta_0 v \cos \theta - \omega_0) t} e^{i\beta_0 z_0}. \quad (5)$$

From the definition of the Fourier transform [41]

$$G(\omega) = \int_{-\infty}^{\infty} g(t) e^{i\omega t} dt \quad (6)$$

and the shift and modulation theorems [42], the spectrum of (4) is given by [43]

$$G(\vec{r}_0, \omega) = \frac{2 \cos \left[\frac{|y_0|}{v \sin \theta} \sqrt{(\alpha v \sin \theta)^2 - (\omega + \beta_0 v \cos \theta - \omega_0)^2} \right]}{\sqrt{(\alpha v \sin \theta)^2 - (\omega + \beta_0 v \cos \theta - \omega_0)^2}} \cdot e^{-i \frac{x_0}{v \sin \theta} (\omega + \beta_0 v \cos \theta - \omega_0) + i\beta_0 z_0}, \quad (7)$$

where

$$|\omega - (\omega_0 - \beta_0 v \cos \theta)| < \alpha v \sin \theta. \quad (8)$$

For other ω that do not satisfy (8), $G(\vec{r}_0, \omega) \equiv 0$. This means that the spectrum of the received signal (see (4)) has a finite bandwidth where the boundaries and the central frequency of the spectrum are related to the velocity, \vec{v} . In either (5) or (7), it is seen that the axial distance, z_0 , appears only in the constant phase term, $e^{i\beta_0 z_0}$, and does not affect the magnitude or the

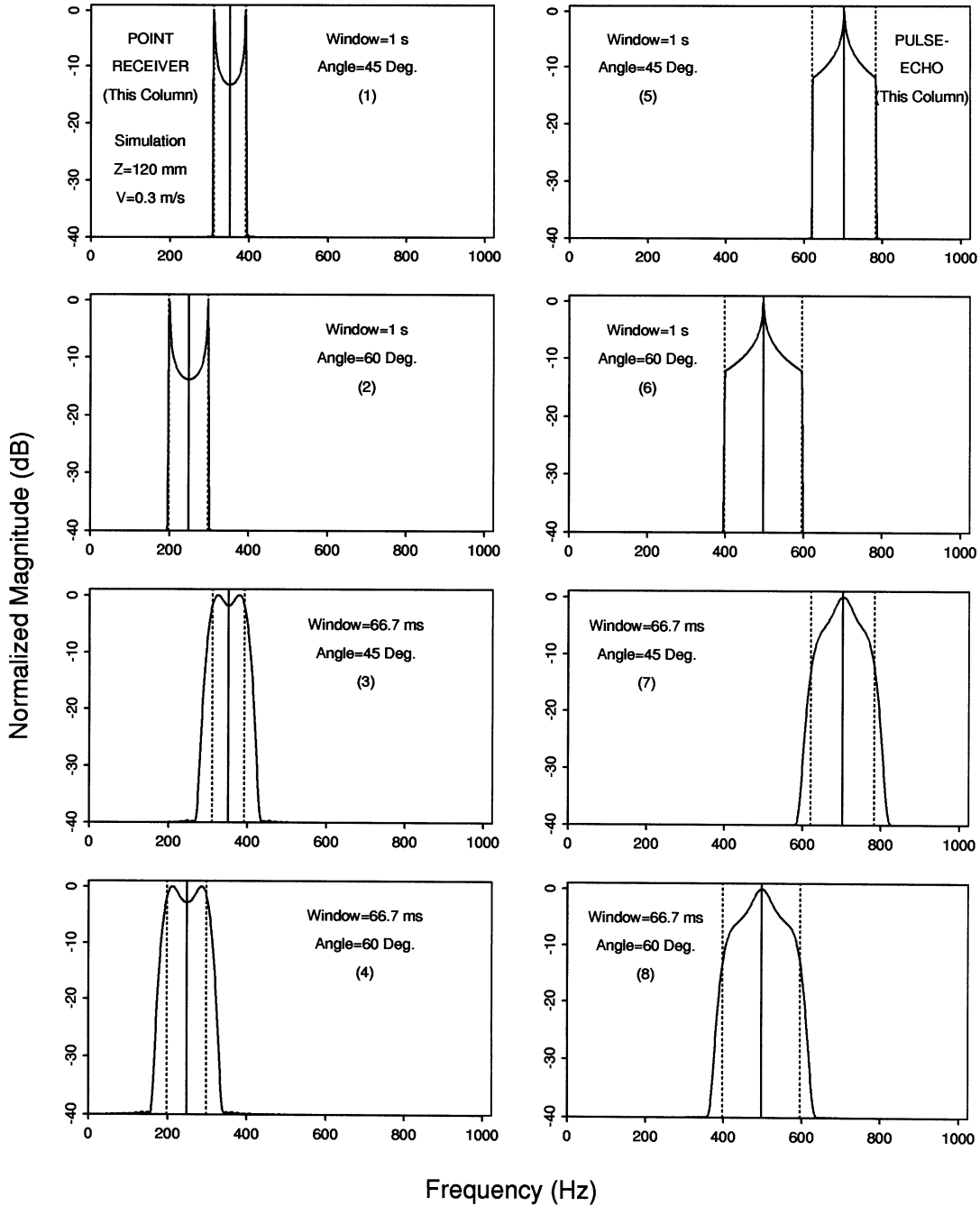


Fig. 2. Simulated Doppler spectra of a moving point receiver (one-way) (Panels (1) to (4)) and a point scatterer (backscattered) (Panels (5) to (8)) at the plane, $y = 0$, in the Bessel beam with the scaling factor, $\alpha = 1202.45 \text{ m}^{-1}$, and frequency of 2.5 MHz. The point was located at $x_0 = 0$ when $t = 0$. The upper and lower 4 panels are the spectra obtained with the time window, $t_1 = 1 \text{ s}$ and 66.7 ms , respectively. The time interval was $[-t_1/2, t_1/2]$ and was weighted with a Blackman window. The panels in the first and the third rows were obtained with the Doppler angle of 45 degrees, while the panels in the second and the fourth rows were obtained at 60 degrees. The velocity and the axial distance, z_A (see Fig. 1), of the point, P_0 , were 0.3 m/s and 120 mm, respectively. At this velocity, the moving distance of the point was 300 mm and 20 mm for $t_1 = 1 \text{ s}$ and 66.7 ms , respectively. The vertical bars show the theoretical prediction of the lower and upper boundaries (dotted lines) and the frequency shift (full line) of the spectra (see (9) to (11) for a moving point receiver, and (24) and (25) for a point scatterer).

shape of the Doppler spectrum. This means that the estimation and of the velocity will not be influenced by the distance of the point receiver if a perfect Bessel beam is used.

From (8) one obtains the lower and upper boundaries of the spectrum (abrupt cut-offs in the spectrum (Figs. 2(1) and (2))),

$$\omega_l = \omega_c - \omega_b/2 \quad (9)$$

respectively, where

$$\omega_h = \omega_c + \omega_b/2, \quad (10)$$

$$\omega_c = \omega_0 + \Delta\omega \quad (11)$$

is the shifted central frequency,

$$\Delta\omega = -\beta_0 v \cos \theta = \beta_0 v \cos \theta_1 \quad (12)$$

is the frequency shift (see (8)), and

$$\omega_b = 2\alpha v \sin \theta = 2\alpha v \sin \theta_1 \quad (13)$$

is the bandwidth of the spectrum (Figs. 2(1) and (2)), where $\theta_1 = \pi - \theta$ (Fig. 1(a)) (for $\theta_1 < \pi/2$, the velocity has a component that is toward the transducer and thus the frequency shift, $\Delta\omega$, is positive). Note that the bandwidth, ω_b , is not a function of the frequency of the beam, and the Doppler spectrum has the same shape ((8) and (12)) at any central frequency, ω_c . This is different from that of a conventional focused beam where the bandwidth of the Doppler spectrum is a linear function of the central frequency [9].

Once we measure the frequency shift, $\Delta\omega$, and the bandwidth, ω_b , the velocity of the point receiver and the angle between the velocity and the beam axis can be calculated

$$v = \sqrt{\left(\frac{\omega_b}{2\alpha}\right)^2 + \left(\frac{\Delta\omega}{\beta_0}\right)^2}, \quad (14)$$

and

$$\theta = \tan^{-1}\left(-\frac{\omega_b \beta_0}{2\alpha \Delta\omega}\right), \quad \text{when } \Delta\omega < 0, \quad (15)$$

or

$$\theta_1 = \tan^{-1}\left(\frac{\omega_b \beta_0}{2\alpha \Delta\omega}\right), \quad \text{when } \Delta\omega \geq 0. \quad (16)$$

At $\theta = 0$, the Doppler spectrum (see (7)) is not varied. The Doppler spectrum in this case must be obtained from the Fourier transform of (4) with $\theta = 0$ directly,

$$G(\vec{r}_0, \omega) = 2\pi J_0\left(\alpha\sqrt{x_0^2 + y_0^2}\right)\delta(\omega - (\omega_0 - \beta_0 v))e^{i\beta_0 z_0}. \quad (17)$$

Since $\theta = 0$, the point receiver is moving directly away from the source (Fig. 1(a)) resulting a negative frequency shift, $-\beta_0 v$, from ω_0 . The magnitude of the spectrum is a function of the position of the point receiver $\left|2\pi J_0\left(\alpha\sqrt{x_0^2 + y_0^2}\right)\right|$ and the Doppler spectrum has a zero bandwidth (see the δ -function in (17)).

If $\theta = 90^\circ$, the Doppler spectrum can be obtained directly from (7)

$$G(\vec{r}_0, \omega) = \frac{2 \cos \left[\frac{|y_0|}{v \sin \theta} \sqrt{(\alpha v)^2 - (\omega - \omega_0)^2} \right]}{\sqrt{(\alpha v)^2 - (\omega - \omega_0)^2}} \cdot e^{-i \frac{\pi \alpha}{v} (\omega - \omega_0) + i \beta_0 z_0}, \quad (18)$$

and one sees no shift in the central frequency but a maximum bandwidth of the Doppler spectrum, $\omega_b = 2\alpha v$.

Equation (7) has the following property

$$|G(\vec{r}_0, \omega)| \leq |G(\vec{r}_0, \omega)|_{y_0=0}, \quad (19)$$

where

$$|G(\vec{r}_0, \omega)|_{y_0=0} = \begin{cases} \frac{2}{\sqrt{(\alpha v \sin \theta)^2 - (\omega + \beta_0 v \cos \theta - \omega_0)^2}}, & |\omega + \beta_0 v \cos \theta - \omega_0| < \alpha v \sin \theta \\ 0, & \text{otherwise} \end{cases} \quad (20)$$

is obtained from (7) with $y_0 = 0$. This implies that the Doppler spectrum for a moving point receiver is under the curve defined by (20) which is peaked at the spectrum boundaries and has a minimum at the central frequency, $\omega_0 - \beta_0 v \cos \theta$ (Figs. 2(1) and (2)). The peaks at the boundaries makes it easy to determine the bandwidth of the spectrum and thus the Doppler angle (see (15)).

It is noted from (4) that if $|y_0| > 0$, the maximum amplitude of the received signal will decrease rapidly and monotonically with $|y_0|$. This means that the signals received off the plane, $y = 0$, may be negligible.

C. Doppler Spectrum from a Moving Point Scatterer

If the Bessel transducer in Fig. 1 is used as both a transmitter and a receiver [25], the received signal that is backscattered from a point scatterer is given by [44]

$$g_b(\vec{r}_0, t) = \left[J_0 \left(\alpha \sqrt{(x_0 + vt \sin \theta)^2 + y_0^2} \right) e^{i\beta_0 z_0} \right]^2 \cdot e^{i(2\beta_0 v \cos \theta - \omega_0)t} \quad (21)$$

where the subscript "b" represents "backscattered". The Doppler spectrum (Figs. 2(5) and (6)) of the received signal is the Fourier transform of (21)

$$G_b(\vec{r}_0, \omega) = [G_1(\vec{r}_0, \omega_1) * G_1(\vec{r}_0, \omega_1)]|_{\omega_1 = \omega + 2\beta_0 v \cos \theta - \omega_0}, \quad (22)$$

where "*" represents the convolution with respect to ω_1 , and

$$G_1(\vec{r}_0, \omega_1) = \frac{2 \cos \left[\frac{|y_0|}{v \sin \theta} \sqrt{(\alpha v \sin \theta)^2 - \omega_1^2} \right]}{\sqrt{(\alpha v \sin \theta)^2 - \omega_1^2}} \cdot e^{-i \frac{\pi \alpha}{v \sin \theta} \omega_1 + i \beta_0 z_0}, \quad (23)$$

which is the Fourier transform of the term inside the square bracket in (21) and is similar to (7).

Because $G_1(\vec{r}_0, \omega_1)$ is convolved with itself in (22), the bandwidth of the backscattered Doppler signal is doubled from that of the signal of a moving point receiver (see (13)), i.e.,

$$\omega_{bb} = 4\alpha v \sin \theta. \quad (24)$$

The central frequency of the backscattered Doppler signal can be obtained from the expression of ω_1 in (22), i.e.,

$$\omega_{cb} = \omega_0 - 2\beta_0 v \cos \theta. \quad (25)$$

The equations for calculating the lower and upper boundaries of the backscattered Doppler spectrum are the same as (9)

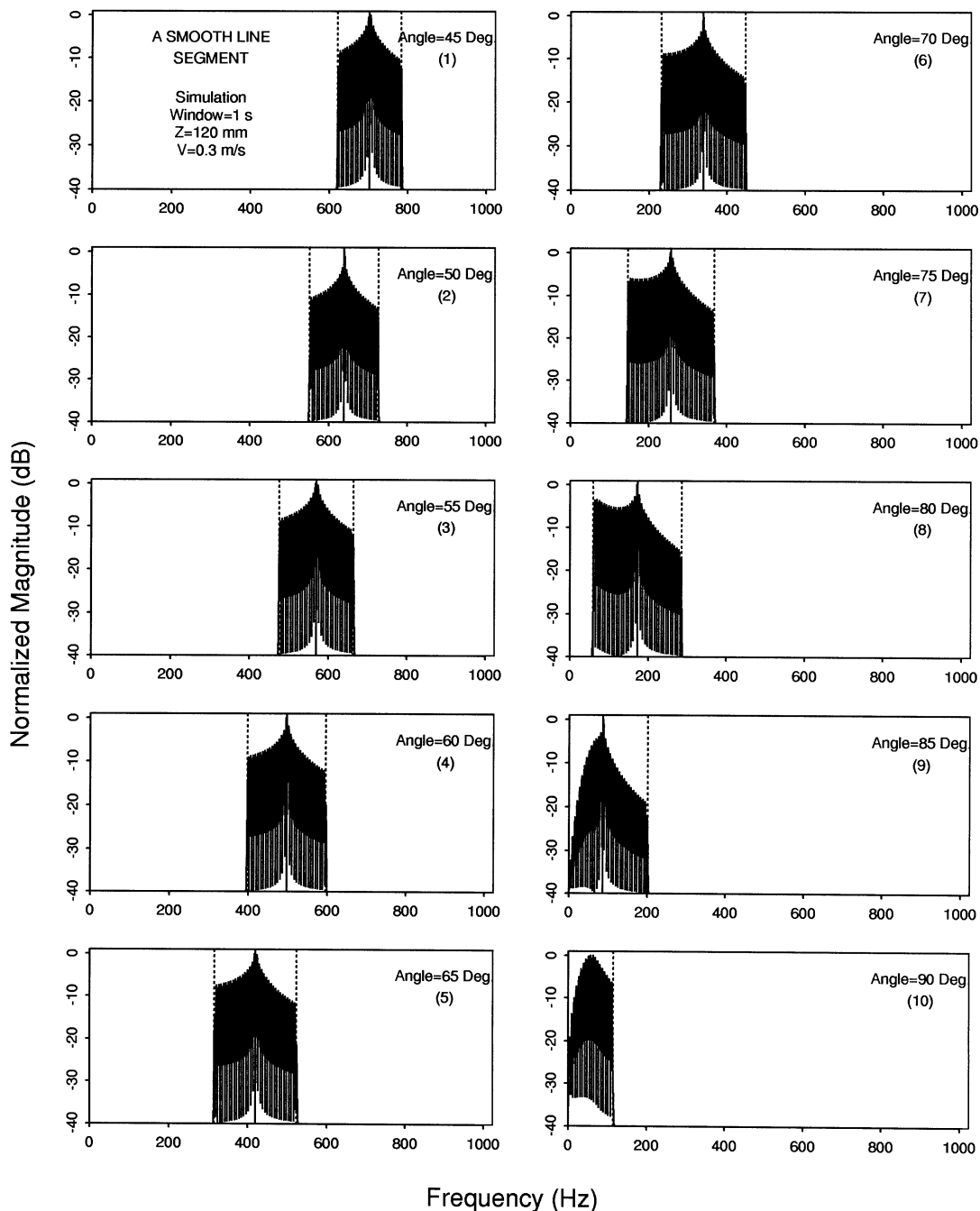


Fig. 3. Simulated Doppler spectra of the backscattered signals from a moving smooth line segment of length of 50 mm (see Fig. 1) in the Bessel beam described in Fig. 2. The line segment was in the plane, $y = 0$. Its velocity was 0.3 m/s and the axial distance, z_A , was 120 mm. A larger Blackman-weighted time window, $t_1 = 1$ s, as in Fig. 2 was applied to the backscattered signals. Panels (1) to (10) correspond to the Doppler angle of 45 to 90 degrees with an increment of 5 degrees. The spectra at 85 and 90 degrees were distorted because a 75 Hz wall filter (high-pass filter) was added. The vertical bars show the theoretical prediction of the lower and upper boundaries (dotted lines) and the frequency shift (full line) of the spectra (they are the same as those of a point scatterer in Fig. 2 and are obtained from (24) and (25)).

and (10). However, ω_b and ω_c in those equations need to be replaced with ω_{bb} and ω_{cb} in (24) and (25).

D. Doppler Spectrum from a Moving Line Segment

For a smooth line that is infinitely long and moves in the direction of the line, there will be no Doppler shift. However, if the line has a finite length, one will see the motion of the end points of the line and thus may obtain Doppler spectrum. In this case, we found an interesting spectrum that is composed

of three peaks corresponding almost exactly to the central frequency, and the lower and upper boundaries of the spectrum (Fig. 4). This might be used to detect the velocity of a smooth javelin in sports or a missile.

If point scatterers are uniformly distributed in a line segment (Fig. 1(b)) of length L , the backscattered signal is an integration of (21)

$$g_{Lb}(y_0, t) = e^{i(2\beta_0 v \cos \theta - \omega_0)t}$$

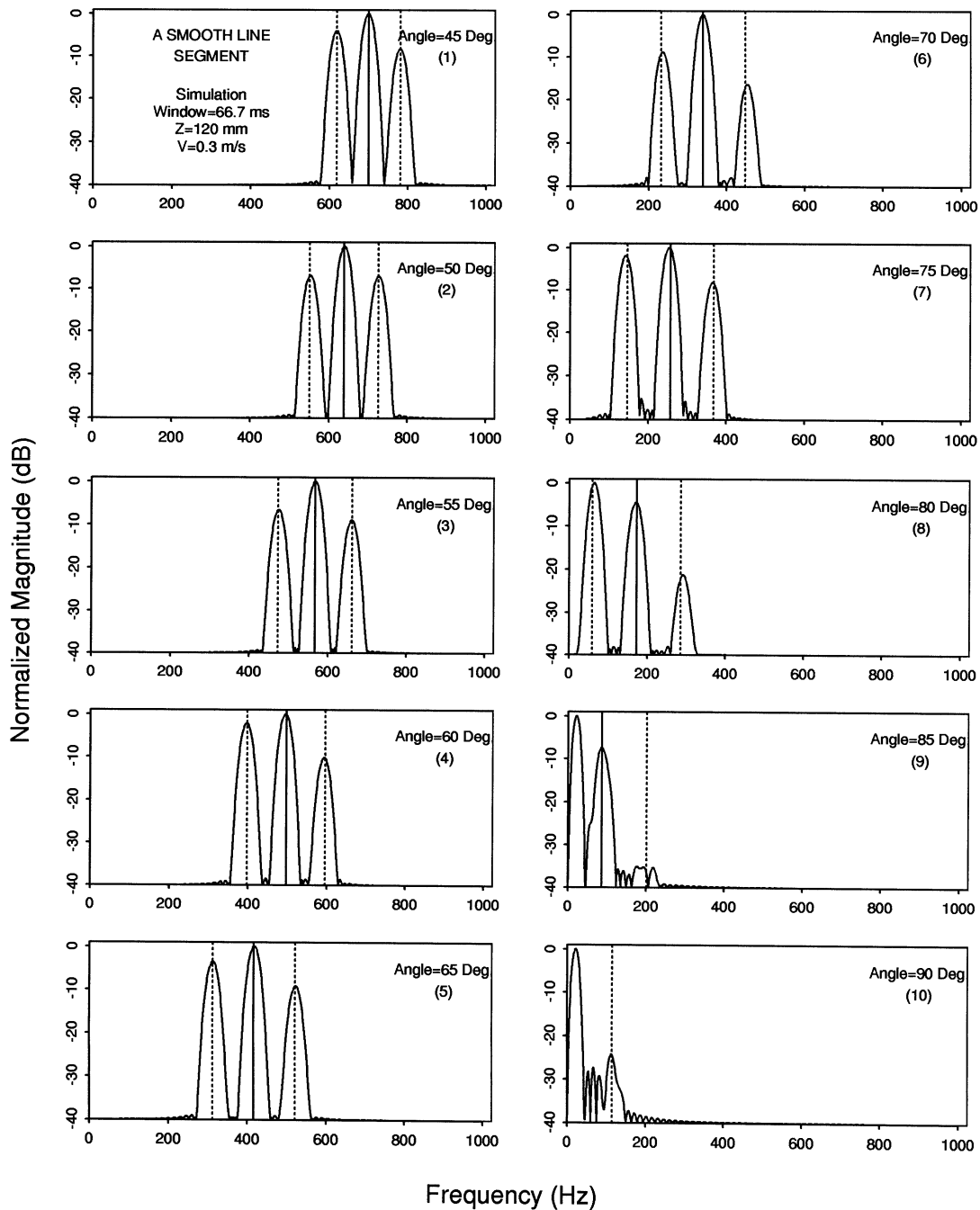


Fig. 4. Simulated under the same conditions as those of Fig. 3, except that a smaller Blackman weighted time window, $t_1 = 66.7$ ms, was applied. The three peaks in the spectra indicate clearly the lower and upper boundaries and frequency shift of the spectra and compare very well with the theoretical prediction.

$$\int_{-(L/2)\sin\theta}^{(L/2)\sin\theta} \left[J_0 \left(\alpha \sqrt{(x_0 + vt \sin\theta)^2 + y_0^2} \right) e^{i\beta_0 z_0} \right]^2 dx_0 \quad (26)$$

where the subscript “L” means “line segment”, $z_0 = z_A + z'$, z_A is a constant (Fig. 1(a)), and $z' = x_0 \cot\theta$. If θ is very small, the integration in (26) needs to be evaluated over z' , with the formula $x_0 = z' \tan\theta$, and the lower and upper limits of the integration are $-(L/2)\cos\theta$ and $(L/2)\cos\theta$,

respectively. The Doppler spectrum of (26) is given by

$$G_{Lb}(y_0, \omega) = \mathcal{F}\{g_{Lb}(y_0, t)\}, \quad (27)$$

which is the Fourier transform of $g_{Lb}(y_0, t)$ with respect to t (Figs. 3 and 4). As $L \rightarrow \infty$, the Doppler signal is weakened and will eventually disappear. This is because the end points of the line move to infinite distance from the center of the beam.

E. Doppler Spectrum from a Line of Moving Random Scatterers

In a thin blood vessel, the red blood cells can be modeled as a line of moving random scatterers (Fig. 1(c)). In this case,

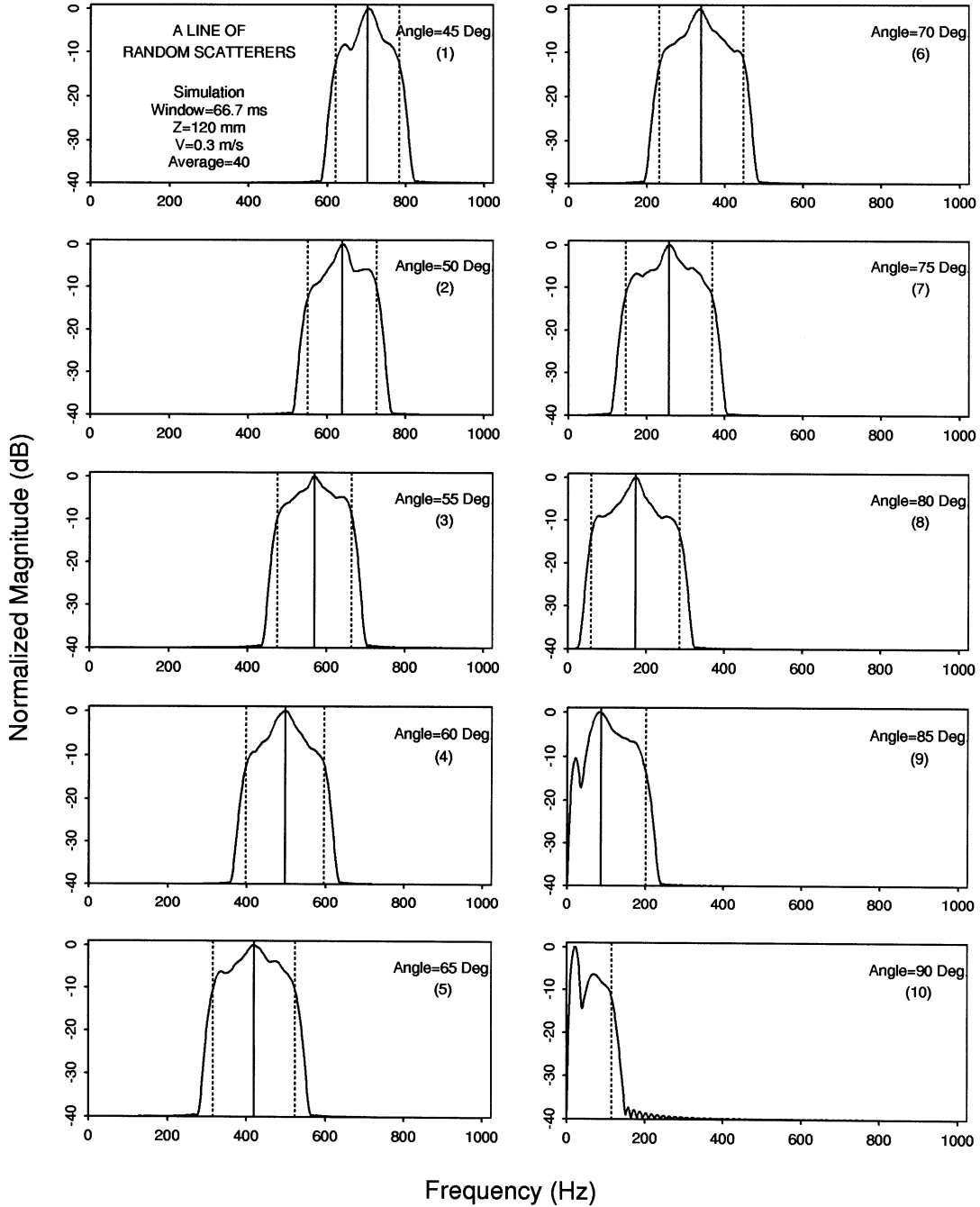


Fig. 5. Simulated under the same conditions as those of Fig. 4, except that the moving smooth line segment was replaced with a line of moving random scatterers. 2048 scatterers were positioned randomly along the 50 mm line (Fig. 1(c)) with a uniform distribution. The spectra were obtained by averaging the magnitudes of 40 independent Doppler spectra from lines of moving random scatterers.

(26) must be evaluated with a summation

$$g_{LRb}(y_0, t) = e^{i(2\beta_0 v \cos \theta - \omega_0)t} \cdot \sum_j \left[J_0 \left(\alpha \sqrt{(x_{0j} + vt \sin \theta)^2 + y_0^2} \right) e^{i\beta_0 z_{0j}} \right]^2 \quad (28)$$

where the subscript “R” means “random,” j is an index of the random scatterers, $z_{0j} = z_A + z'_j$, and $z'_j = x_{0j} \cot \theta$. The Doppler spectrum of the signal from a line of moving random

scatterers is the Fourier transform of (28) with respect to time t , i.e., $G_{LRb}(y_0, \omega) = \mathcal{F}\{g_{LRb}(y_0, t)\}$.

III. SIMULATION

In the following simulation, we assume that a perfect Bessel beam ((1)) is used, where the scaling factor, α , speed of sound, c , and frequency, ω_0 , are 1202 m^{-1} , 1500 m/s , and 2.5 MHz , respectively. We also assume that the objects are moving in the plane $y = 0$. In addition, we ignore the modulation term, $e^{-i\omega_0 t}$, that shifts the Doppler spectrum by the carrier frequency, ω_0 (consider only the frequency components caused

by motion). To avoid abrupt truncation in time, a Blackman window [42] of duration, $[-t_1/2, t_1/2]$, and peaked at $t = 0$ is multiplied with the received signal before taking the Fourier transform. The sampling frequency is 2048 Hz and the total samples for the digital Fourier transform (DFT) [42] is 2048. This means that the frequency resolution of the spectrum is 1 Hz. The low frequency components of the spectrum that correspond to the slow motion of objects are suppressed by a 75 Hz wall filter (a half-width Blackman window that is added to the frequency components that are lower than 75 Hz). It is noted that the lateral axes of the Doppler spectra in all the figures in this paper represent the shifted frequency from ω_0 and the Doppler angles are referred to θ_1 in Fig. 1, which gives a positive frequency shift.

The magnitude of the Doppler spectra ((7) or (20)) of the signal from a moving receiver located in the plane, $y = 0$, with the sampling time, $t_1 = 1s$, is shown in Figs. 2(1) ($\theta_1 = 45^\circ$) and 2(2) ($\theta_1 = 60^\circ$) (assume that at $t = 0$, the receiver is at $x_0 = 0$). For a shorter sampling time, $t_1 = 66.7 ms$, which corresponds to a displacement of 20 mm of the receiver when moving at a velocity of 0.3 m/s, the Doppler spectra are blurred (Figs. 2(3) ($\theta_1 = 45^\circ$) and 2(4) ($\theta_1 = 60^\circ$)). The magnitude of the Doppler spectra of the signal (see (21)) backscattered from a moving point scatterer is shown in Figs. 2(5) to 2(8) that correspond to Figs. 2(1) to 2(4), respectively.

The magnitude of the Doppler spectra of the signal (see (26)) backscattered from a moving smooth line segment (Fig. 1) is shown in Figs. 3 and 4, which correspond to the time window, $t_1 = 1s$ and $66.7 ms$, respectively. At $t = 0$, the line segment is centered at $x_0 = 0$ (Fig. 1(b)). It is interesting to note that with the smaller time window (Fig. 4), the three peaks in the spectra coincide almost exactly with the theoretical prediction of the frequency shift, lower and upper boundaries (calculated from (24) and (25)), respectively. Even with a larger window (Fig. 3), the central peak and the shoulders of the spectra are predicted very well by the theory. For the signal backscattered from a line of moving randomly distributed scatterers (see (28)), the shape of the spectrum may also be random. Therefore, to obtain a meaningful spectrum, the magnitude of a number of independent Doppler spectra must be averaged. Magnitudes of 40 Doppler spectra were averaged from moving random scatterers and are shown in Fig. 5, where a smaller time window, $t_1 = 66.7 ms$, is used.

IV. EXPERIMENT

To verify the theoretical analysis, we designed a Doppler flow phantom (Fig. 6) [45]. A thin sewing thread [7] (about 0.1 mm in diameter) was mounted on the phantom and was used as a line of moving random scatterers. A 10-element, 50 mm diameter, 2.5 MHz central frequency annular array transducer [24] was used to produce either a Bessel beam (with the scaling factor of $\alpha = 1202.45 m^{-1}$) or a focused Gaussian beam (the full width at half maximum (FWHM) of the aperture weighting is 25 mm and the focal length is 120 mm (with a plexiglass lens)) [25]. The backscattered signals from the sewing thread were received with the same transducer, weighted the same

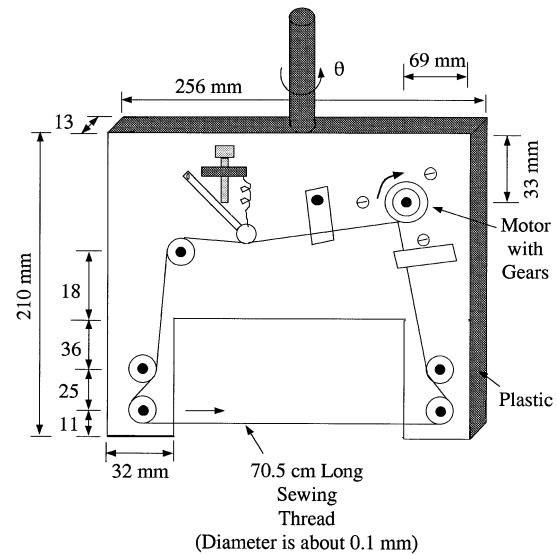


Fig. 6. A Doppler phantom made in our laboratory. A sewing thread of about 70.5 cm long and 0.1 mm in diameter was moved by a DC motor. The speed of the motor was controlled by the DC voltage. The position of the phantom was adjusted so that the part of the thread on the bottom of the phantom passes through the axis (in the plane $y = 0$) of the Bessel beam ($\alpha = 1202.45 m^{-1}$) or the focused Gaussian beam (FWHM = 25 mm at the transducer surface and the focal length $F = 120$ mm (with a plexiglass lens)) that was produced by a 10-element, 50 mm diameter, and 2.5 MHz annular array. The phantom can be rotated around the holding rod to adjust the Doppler angle. The beams were perpendicular to the figure.

way as it was in transmit. The position of the phantom was adjusted so that the sewing thread passed through the center of the beams (the sewing thread was in the plane $y = 0$). The sewing thread was driven by a DC motor and its velocity was controlled by adjusting the DC voltage applied to the motor. The phantom can be rotated around its axis to adjust the Doppler angle, θ_1 (Fig. 1).

A block diagram of the experiment system is shown in Fig. 7. In the experiment, a 2.5 MHz, 20 μs tone-burst produced by a polynomial waveform synthesizer (ANALOGIC DATA 2045) was amplified to drive the transducer. The first and the last 5 μs of the tone-burst were weighted by a rising and falling Blackman window. The weighting reduces the sidelobes of the spectrum dramatically while maintaining the narrow band characteristics of the tone-burst.

To obtain a demodulated backscattered signal, only one datum was acquired by the A/D converter for each transmission of the tone-burst. The delay time between the transmission and the datum acquisition was fixed. If the object that backscatters the incident wave does not move, the acquired datum from each transmission will be the same (no frequency shift). However, if the object moves at a constant speed towards the transducer, the received tone-burst will progressively shift forward in time for each transmission. This change of received data contains the information of the motion. As long as the transmission triggering frequency (pulse repetition frequency or PRF) is high enough so that no aliasing occurs (PRF = 2048 Hz in the experiment), the velocity and the Doppler angle can be estimated from the Doppler spectrum ((14) and (16)).

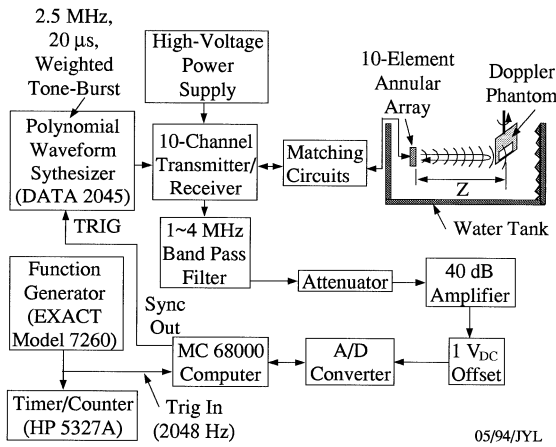


Fig. 7. A block diagram of the Doppler experiment. A polynomial waveform synthesizer (DATA 2045) produced a 2.5 MHz, 20 μ s, and Blackman-window weighted tone-burst that was amplified to drive the annular array transducer to produce either a Bessel or focused Gaussian beam. Echoes received were amplified, aperture weighted in the same way as in the transmit, and digitized by an A/D converter at a fixed delay time that was chosen to sample a point at the middle of the tone-burst. Only one sample was acquired for each transmission of the tone-burst. Trigger pulses for beam transmissions were produced by a function generator (EXACT 7260) at 2048 Hz (the pulse repetition frequency) that was monitored by the Timer/Counter (HP 5327A).

To match the simulation (Fig. 5), magnitudes of about 40 independent Doppler spectra from the sewing thread were averaged and the Blackman time window of the duration, $[-t_1/2, t_1/2]$, where $t_1 = 66.7$ ms, was applied to the signals before the Fourier transform.

V. RESULTS

The magnitude of the Doppler spectra of the backscattered signals from a line of moving random scatterers (sewing thread) is shown in Figs. 8 and 9, for the Bessel and focused Gaussian beams (see last section), respectively. The spectra are obtained at two depths (120 mm and 150 mm). The spectrum obtained with the focused Gaussian beam shows more variation with depth. The signals were processed in the same manner described in the last section.

To demonstrate the Doppler spectra of the backscattered signal from a blood vessel that has a parabolic velocity distribution, we placed the sewing thread at an axial distance of $z = z_A = 120$ mm, and obtained the backscattered signal from 11 positions from -5 mm to $+5$ mm in 1 mm steps. Here we assume that the blood vessel is very thin in the y direction and is located in the plane, $y = 0$. This assumption is reasonable because the amplitude of the Bessel function in (4) or (21) drops quickly as $|y_0|$ increases. The velocity of the sewing thread was varied using the following parabolic formula

$$v = v_{max} \left(1 - \left(\frac{z - z_A}{a_b} \right)^2 \right), \quad |z - z_A| \leq a_b \quad (29)$$

where v_{max} is the maximum velocity of the red blood cells (0.3 m/s) and a_b is the radius of the blood vessel (6 mm). From this equation, it is seen that each velocity corresponds to two

depths (except at $v = v_{max}$). Therefore, the backscattered signals from two depths are superposed coherently (rf summation) to represent the signal at one velocity. The Doppler spectra of the signals from the above 6 different velocities are shown in Panels (1) to (6) of Fig. 10. To obtain the spectrum of signals from the entire vessel, the rf signals for the 6 velocities are summed (see Panel (7) of Fig. 10).

VI. DISCUSSION

From the simulations and the experiments, we have shown that the Doppler spectra obtained with Bessel beams have shoulders that are different from those obtained with conventional focused beams [9]. These shoulders indicate clearly the bandwidth of the Doppler spectrum and correspond to the theoretical prediction very well. The central frequency can be either determined from the peak of the spectrum (for backscattered signals) or calculated from the shoulders. Therefore, from the shoulders, the velocity of object and the Doppler angle can be estimated if the object is moving in a constant speed during the data acquisition time, t_1 . Because the shoulders are relatively high in amplitude (around -10 -dB of the peak of the Doppler spectrum (for backscattered signals)), their identification is less sensitive to noise than when using a conventional focused beam where there is no shoulder at all. This may increase the accuracy of the estimation of magnitude and angle of velocity. In addition, because the Bessel beam has a large depth of field even if it is produced with a finite aperture (see (2)) [17], [24], [25], its Doppler spectra have less variation with depth as compared to a focused Gaussian beam (Figs. 8 and 9).

Although the experimental study on the moving sewing thread has shown the major features of the Doppler spectrum predicted by the theory and simulation, it is preliminary. The Doppler spectrum obtained from the experiment contains a broadband noise (Figs. 8 to 10) produced from our multi-channel receiver. The differences between the results of a moving thread experiment with the Bessel beam (Fig. 8) and the simulation of a line of moving random scatterers (Fig. 5) are caused by the aperture weighting errors due to high cross talk among our transmit amplifiers, the truncation of the Bessel beam to a finite diameter, say, 50 mm, the specular reflections from trapped air bubbles and regular patterns in the thread, and the nonuniform thickness of the thread. The deviation of the shape of the Doppler spectrum (Fig. 9) from that of Gaussian is also caused by the nonideal Gaussian beam due to the aperture weighting errors.

The simulation demonstrated that the Doppler spectrum of signal from a moving receiver has only shoulders and no central peak (Figs. 2(1) to 2(4)) producing more distinct shoulders. In a pulse-echo system, such Doppler spectra can be produced by using a Bessel beam in transmit and an unfocused planar aperture in receive or vice versa (the role of the unfocused planar receiver or transmitter is to shift the Doppler spectrum obtained with the Bessel beam by about $f_0 \frac{v}{c} \cos \theta_1$, where f_0 is the central frequency of the transmitting beam). However, the broad spatial response of the unweighted planar

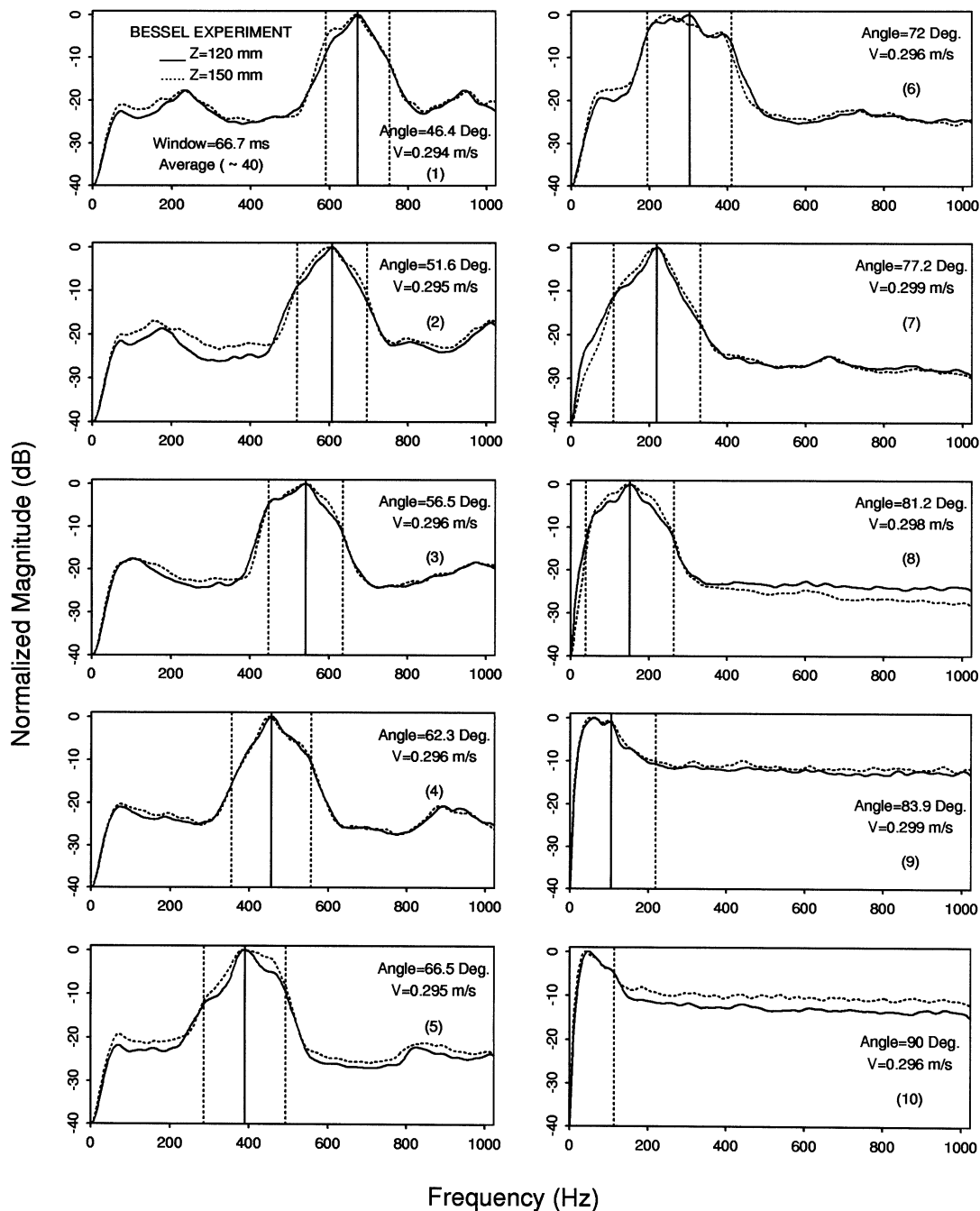


Fig. 8. Measured Doppler spectra of the backscattered signals for a moving sewing thread (Fig. 6) that represents a line of moving random scatterers. The thread passed through the axis (in the plane $y = 0$) of the Bessel beam that was produced by the transducer described in Fig. 6, and was at two axial distances, $z_A = 120 \text{ mm}$ (full line) and 150 mm (dotted line), respectively. A 2.5 MHz, 20 μs , and Blackman-weighted tone-burst was used to excite the transducer and the received signals were also weighted with the Blackman window with the time duration, $t_1 = 66.7 \text{ ms}$. The velocity of the thread was obtained by measuring the time of the node of the thread passing through a reference point in space and dividing the length of the thread with the time (10 revolutions were used to reduce the error). The Doppler angle in each panel was calculated from the spectrum and was roughly from 45 (Panel (1)) to 90 (Panel (10)) degrees at an increment of 5 degrees. A 75 Hz wall filter was added to the spectra to reduce the large signals from the slow motion of the thread. The vertical bars show the theoretical predication of the lower and upper boundaries (dotted lines) and the frequency shift (full line) of the spectra (calculated from (24) and (25)).

aperture may reduce the spatial resolution and increase the sidelobes.

Estimation of the velocity distribution in a blood vessel is important for flow estimation. The current method is to choose a very small range cell (short pulse duration) and place the range cell within different positions of a blood vessel to obtain a rough estimation of the velocity distribution. It is apparent

that the smaller the range cell is, the broader the bandwidth of the impinging beams will be and thus the less accurate the velocity estimation. Therefore, it is desirable that one could estimate the velocity distribution from the Doppler spectrum with a larger range cell. The Doppler spectrum obtained with the Bessel beam has the feature that the spectrum of each velocity component has shoulders and the bandwidth of the

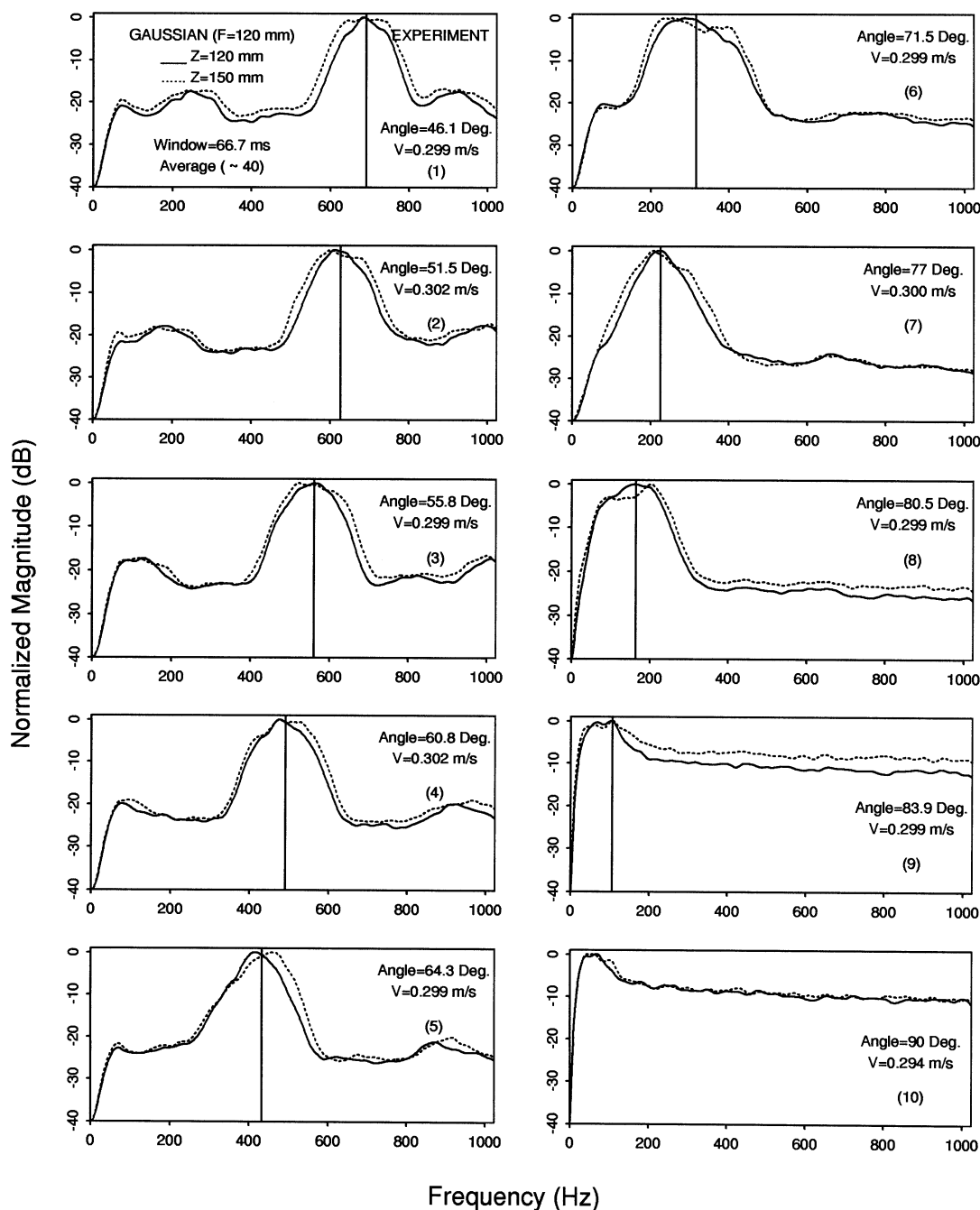


Fig. 9. Doppler spectra obtained with the same procedures as those in Fig. 8, except that a focused Gaussian beam (FWHM = 25 mm at the transducer surface and the focal length $F = 120$ mm (with a plexiglass lens)) was used. The vertical bars represent the shift of the central frequency.

spectrum depends only on the velocity (Fig. 10). Thus the spectrum from a group of scatterers traveling at different speeds will be a summation of nonorthogonal basis functions. This might be of help in the estimation of velocity distributions (an inverse problem) and could be studied in the future.

For medical applications, more complicated situations such as the use of short pulses (broadband probing signals), shorter sampling time (smaller number of samples in color flow mapping [6]), and existence of pulsatile flow will have to be considered. The solution to these problems might be a trade-off between the accuracy of the velocity estimation and the above parameters. Time domain velocity estimation might be a better approach to some of these problems [46].

VII. CONCLUSION

Limited-diffraction beams have a large depth of field. They could be applied to medical imaging [24]–[26], tissue characterization [27], [28], and nondestructive evaluation (NDE) of materials [29]. This paper has shown that limited-diffraction beams, especially, the Bessel beam, can also be applied to velocity estimation using the Doppler effect. Application of the Bessel beam to velocity estimation has the advantage that its Doppler spectrum has little depth dependence and has distinct shoulders that may increase the accuracy of the velocity magnitude and angle estimates in noisy environments, as compared to conventional focused beams. The distinct

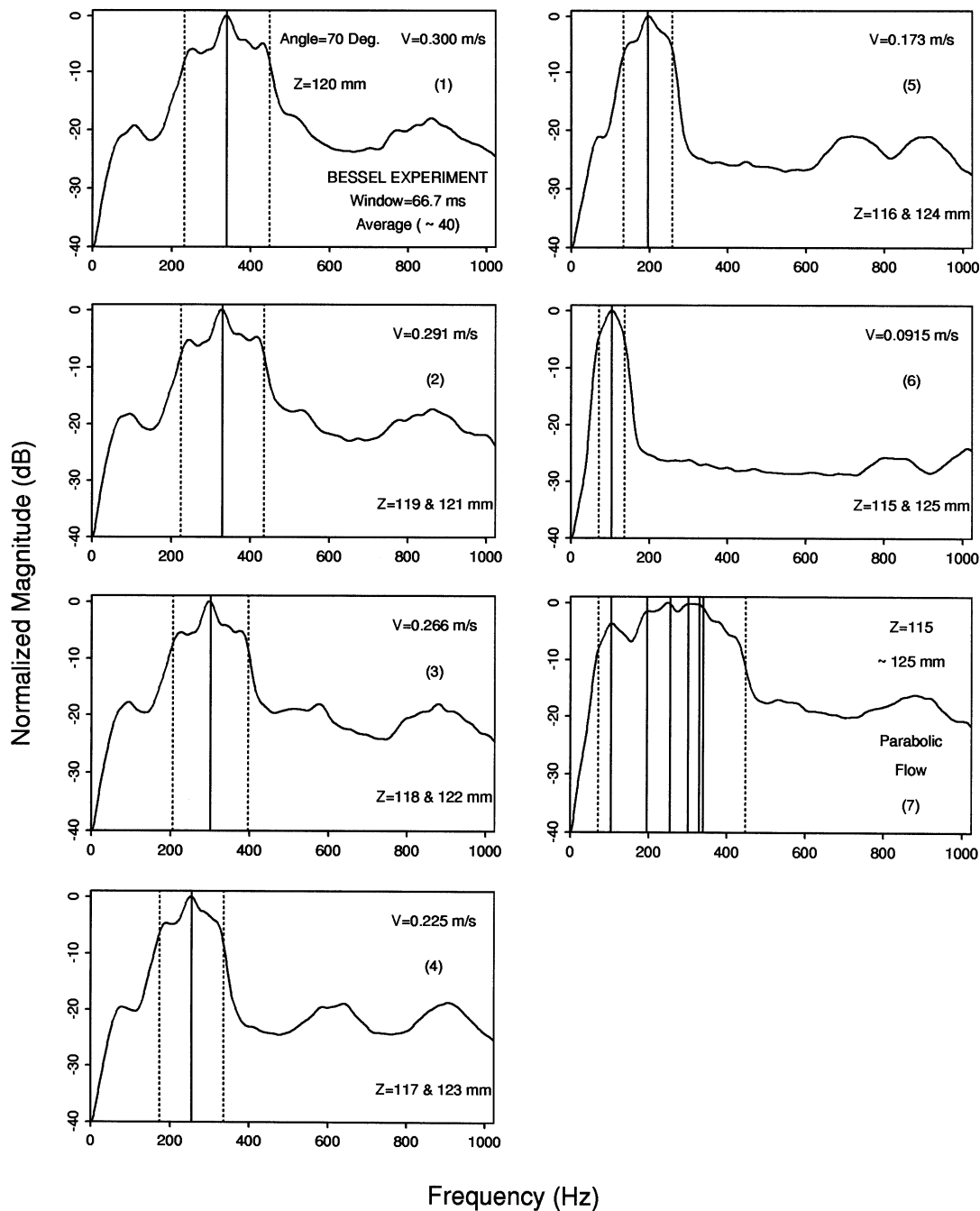


Fig. 10. Measured Doppler spectra of the backscattered signals for a vessel of parabolic flow (the velocity distribution on a cross section of the vessel is a parabolic function) in the Bessel beam produced by the transducer described in Fig. 6. The vessel was assumed to be very thin and located in the plane, $y = 0$, with its center located at the axial distance, $z_A = 120 \text{ mm}$. The diameter of the vessel was 12 mm, and there were only 6 different velocities that span a distance of 10 mm with an increment of 1 mm (except at the center of the vessel, each velocity corresponds to two spatial positions in the parabolic flow). The Doppler angle was 70 degrees. Panels (1) to (6) correspond to 6 velocities in a parabolic velocity distribution, i.e., $v = 0.3, 0.291, 0.266, 0.225, 0.173$, and 0.0915 m/s , respectively. For Panels (2) to (6), the backscattered signals from two positions were summed coherently to obtain the Doppler spectra. The Doppler spectrum of the backscattered signals from the entire vessel is shown in Panel (7) and was obtained by coherently summing the signals of the above 6 panels. The vertical bars show the theoretical prediction of the lower and upper boundaries (dotted lines) of the spectra and the frequency shift (solid lines).

shoulders of the Doppler spectrum produced by the Bessel beam might help in estimating distributions of velocities in blood vessels.

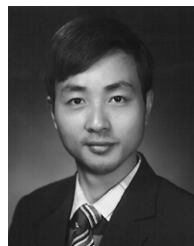
ACKNOWLEDGMENT

The authors thank Mr. Randall R. Kinnick for making the Doppler phantom. The secretarial assistance of Elaine C. Quarve is appreciated.

REFERENCES

- [1] C. Doppler, "Ueber das farbige Licht der Doppelsterne und einiger anderer Gestirne des Himmels," *Abhandlungen der Koniglich Bohmischen Gesellschaft der Wissenschaften*, vol. 2, no. 5, pp. 465–482, 1843.
- [2] E. J. Jonkman, "Doppler research in the nineteenth century," *Ultrasound Med. Biol.*, vol. 6, no. 1, pp. 1–5, Jan. 1980.
- [3] D. L. Franklin, W. Schlegel, R. F. Rushmer, "Blood flow measured by Doppler frequency shift of back-scattered ultrasound," *Sci.*, vol. 134, pp. 564–565, 1961.

- [4] P. N. T. Wells, "A range-gated ultrasonic Doppler system," *Med. Biol. Eng.*, vol. 7, pp. 641–652, 1969.
- [5] J. M. Reid and M. P. Spencer, "Ultrasonic Doppler technique for imaging blood vessels," *Sci.*, vol. 176, pp. 1235–1236, 1972.
- [6] P. A. Magnin, "A review of Doppler flow mapping techniques," in *IEEE 1987 Ultrason. Symp. Proc.*, 87CH2492–7, vol. 2, pp. 969–977, 1987.
- [7] V. L. Newhouse, E. S. Furgason, G. F. Johnson, and D. A. Wolf, "The dependence of ultrasound Doppler bandwidth on beam geometry," *IEEE Trans. Sonic. Ultrason.*, vol. SU-27, pp. 50–59, 1980.
- [8] P. A. J. Bascom, R. S. C. Cobbold, and B. H. M. Roelofs, "Influence of spectral broadening on continuous wave Doppler ultrasound spectra: a geometric approach," *Ultrasound Med. Biol.*, vol. 12, pp. 387–395, 1986.
- [9] V. L. Newhouse, D. Censor, T. Vontz, J. A. Cisneros, and B. B. Goldberg, "Ultrasound Doppler probing of flows transverse with respect to beam axis," *IEEE Trans. Biomed. Eng.*, vol. BME-34, no. 10, pp. 779–789, Oct. 1987.
- [10] D. Censor, V. L. Newhouse, T. Vontz, and H. V. Ortega, "Theory of ultrasound Doppler-spectra velocimetry for arbitrary beam and flow configurations," *IEEE Trans. Biomed. Eng.*, vol. 35, no. 9, pp. 740–751, Oct. 1988.
- [11] V. L. Newhouse and J. M. Reid, "Invariance of Doppler bandwidth with flow axis displacement," in *IEEE 1990 Ultrason. Symp. Proc.*, 1990, vol. 2, pp. 1533–1536.
- [12] P. Tortoli, G. Guidi, V. Mariotti, and V. L. Newhouse, "Experimental proof of Doppler bandwidth invariance," *IEEE Trans. Ultrason., Ferroelec., Freq. Contr.*, vol. 39, no. 2, pp. 196–203, Mar. 1992.
- [13] P. Tortoli, G. Guidi, V. Mariotti, and V. L. Newhouse, "Invariance of the Doppler bandwidth with range cell size above a critical beam-to-flow angle," *IEEE Trans. Ultrason., Ferroelec., Freq. Contr.*, vol. 40, no. 4, pp. 381–386, Jul. 1993.
- [14] J. N. Brittingham, "Focus wave modes in homogeneous Maxwell's equations: transverse electric mode," *J. Appl. Phys.*, vol. 54, no. 3, pp. 1179–1189, 1983.
- [15] R. W. Ziolkowski, "Exact solutions of the wave equation with complex source locations," *J. Math. Phys.*, vol. 26, no. 4, pp. 861–863, Apr. 1985.
- [16] R. W. Ziolkowski, D. K. Lewis, and B. D. Cook, "Evidence of localized wave transmission," *Phys. Rev. Lett.*, vol. 62, no. 2, pp. 147–150, Jan. 1989.
- [17] J. Durnin, "Exact solutions for nondiffracting beams. I. The scalar theory," *J. Opt. Soc. Am.*, vol. 4, no. 4, pp. 651–654, 1987.
- [18] Jian-yu Lu, Hehong Zou, and J. F. Greenleaf, "Biomedical ultrasound beam forming," *Ultrasound Med. Biol.* vol. 20, no. 5, pp. 403–428, July, 1994.
- [19] Jian-yu Lu and J. F. Greenleaf, "Nondiffracting X waves — exact solutions to free-space scalar wave equation and their finite aperture realizations," *IEEE Trans. Ultrason., Ferroelec., Freq. Contr.*, vol. 39, no. 1, pp. 19–31, Jan. 1992.
- [20] ———, "Experimental verification of nondiffracting X waves," *IEEE Trans. Ultrason., Ferroelec., Freq. Contr.*, vol. 39, no. 3, pp. 441–446, May 1992.
- [21] D. K. Hsu, F. J. Margetan, and D. O. Thompson, "Bessel beam ultrasonic transducer: fabrication method and experimental results," *Appl. Phys. Lett.*, vol. 55, no. 20, pp. 2066–2068, Nov. 1989.
- [22] J. A. Campbell and S. Soloway, "Generation of a nondiffracting beam with frequency independent beam width," *J. Acoust. Soc. Am.*, vol. 88, no. 5, pp. 2467–2477, Nov. 1990.
- [23] R. Donnelly, D. Power, G. Templeman, and A. Whalen, "Graphic simulation of superluminal acoustic localized wave pulses" *IEEE Trans. Ultrason., Ferroelec., Freq. Contr.*, vol. 41, no. 1, pp. 7–12, 1994.
- [24] Jian-yu Lu and J. F. Greenleaf, "Ultrasonic nondiffracting transducer for medical imaging," *IEEE Trans. Ultrason., Ferroelec., Freq. Contr.*, vol. 37, no. 5, pp. 438–447, Sept. 1990.
- [25] ———, "Pulse-echo imaging using a nondiffracting beam transducer," *Ultrasound Med. Biol.*, vol. 17, no. 3, pp. 265–281, May 1991.
- [26] Jian-yu Lu, Tai K. Song, Randall R. Kinnick, and J. F. Greenleaf, "In vitro and in vivo real-time imaging with ultrasonic limited diffraction beams," *IEEE Trans. Med. Imag.*, vol. 12, no. 4, pp. 819–829, Dec. 1993.
- [27] Jian-yu Lu and J. F. Greenleaf, "Evaluation of a nondiffracting transducer for tissue characterization," in *IEEE 1990 Ultrason. Symp. Proc.*, 1990, vol. 2, pp. 795–798.
- [28] ———, "Diffraction-limited beams and their applications for ultrasonic imaging and tissue characterization," in *Proc. SPIE*, 1992, vol. 1733, pp. 92–119.
- [29] ———, "Producing deep depth of field and depth-independent resolution in NDE with limited diffraction beams," *Ultrason. Imag.*, vol. 15, no. 2, pp. 134–149, Apr. 1993.
- [30] R. W. Ziolkowski, "Localized transmission of electromagnetic energy," *Phys. Rev. A.*, vol. 39, no. 4, pp. 2005–2033, Feb. 15, 1989.
- [31] R. Donnelly and R. W. Ziolkowski, "Designing localized waves," *Proc. Royal Soc. Lond., A*, vol. 440, pp. 541–565, 1993.
- [32] J. Durnin, J. J. Miceli, Jr., and J. H. Eberly, "Diffraction-free beams," *Phys. Rev. Lett.*, vol. 58, no. 15, pp. 1499–1501, Apr. 1987.
- [33] A. Vasara, J. Turunen, and A. T. Friberg, "Realization of general nondiffracting beams with computer-generated holograms," *J. Opt. Soc. Am. A*, vol. 6, no. 11, pp. 1748–1754, 1989.
- [34] G. Indebetow, "Nondiffracting optical fields: some remarks on their analysis and synthesis," *J. Opt. Soc. Am. A*, vol. 6, no. 1, pp. 150–152, Jan. 1989.
- [35] F. Gori, G. Guattari, and C. Padovani, "Model expansion for J_0 -correlated Schell-model sources," *Optics Commun.*, vol. 64, no. 4, pp. 311–316, Nov. 1987.
- [36] ———, "Bessel-Gaussian beams," *Optics Commun.*, vol. 64, no. 6, pp. 491–495, Dec. 1987.
- [37] K. Uehara and H. Kikuchi, "Generation of near diffraction-free laser beams," *Appl. Physics B*, vol. 48, pp. 125–129, 1989.
- [38] L. Vicari, "Truncation of nondiffracting beams," *Optics Commun.*, vol. 70, no. 4, pp. 263–266, Mar. 1989.
- [39] M. Zahid and M. S. Zubairy, "Directionally of partially coherent Bessel-Gauss beams," *Optics Commun.*, vol. 70, no. 5, pp. 361–364, Apr. 1989.
- [40] S. Y. Cai, A. Bhattacharjee, and T. C. Marshall, "'Diffraction-free' optical beams in inverse free electron laser acceleration," *Nuclear Instruments and Methods in Physics Research, Section A: Accelerators, Spectrometers, Detectors, and Associated Equipment*, vol. 272, no. 1–2, pp. 481–484, Oct. 1988.
- [41] R. Bracewell, *The Fourier Transform and Its Applications*. New York: McGraw-Hill, 1965, ch. 4 and 6.
- [42] A. V. Oppenheim and R. W. Schaffer, *Digital Signal Processing*. Englewood Cliffs, NJ: Prentice-Hall, 1975, ch. 1 and 5.
- [43] I. S. Gradshteyn and I. M. Ryzhik, *Table of Integrals, Series, and Products*. New York: Academic Press, 1980, ch. 6 and 17.
- [44] J.-Y. Lu and J. F. Greenleaf, "A study of sidelobe reduction for limited diffraction beams," in *IEEE 1993 Ultrason. Symp. Proc.*, 1993, vol. 2, pp. 1077–1082.
- [45] A. R. Walker, D. J. Phillips, and J. E. Powers, "Evaluating Doppler devices using a moving string test target," *J. Clin. Ultrasound*, vol. 10, pp. 25–30, Jan. 1982.
- [46] A. Hein and W. D. O'Brien, "Current time-domain methods for assessing tissue motion by analysis from reflected ultrasound echoes—a review," *IEEE Trans. Ultrason., Ferroelec., Freq. Contr.*, vol. 40, no. 2, pp. 84–102, Mar. 1993.



Jian-Yu Lu (M'88) received the B.S. degree in electrical engineering in 1982 from Fudan University, Shanghai, China, the M.S. degree in 1985 from Tongji University, Shanghai, China and the Ph.D. degree from Southeast University, Nanjing, China.

He is currently an Associate Consultant at Biodynamics Research Unit, Department of Physiology and Biophysics, Mayo Clinic and Foundation, Rochester, MN, and he is an Assistant Professor at the Biodynamics Research Unit at the Mayo Medical School. Previously, he was a Research Associate at the Biodynamic Unit, and from 1988 to 1990, he was a Post-Doctoral Research Fellow. Prior to that, he was a faculty member of the Department of Biomedical Engineering, Southeast University, and worked with Professor Yu Wei. His research interests are in acoustical imaging and tissue characterization, medical ultrasonic transducers, and nondiffracting wave transmission.

Dr. Lu is a member of the IEEE UFFC Society, the American Institute of Ultrasound in Medicine, and Sigma Xi.



Xiao-Liang Xu (S'88-M'92) received the B.S. and M.S. degrees from Zhejiang University, Hangzhou, China, in 1982 and 1984, respectively, and the Ph.D. degree from the University of Minnesota, MN, in 1991, all in electrical engineering.

From 1984 to 1986 he was with the Department of Electrical Engineering at Zhejiang University in China. From 1987 to 1991 he was a Research Associate at the University of Minnesota. From 1991 to 1993 he was a Post-Doctoral Fellow at the VA Medical Center and

University of Minnesota, MN. Since 1993 he has been a Research Associate at the Mayo Clinic, Rochester, MN. His research interests include medical imaging systems, image analysis, biomedical signal processing, statistical signal processing, and spectrum analysis.



Hehong Zou received the B.Sc. degree from the Beijing University of Science and Technology, Beijing, China, in 1985, the M.S. degree from the University of Wisconsin, Milwaukee, WI, in 1989, and the Ph.D. degree from the University of Minnesota, Minneapolis, MN, in 1993, all in electrical engineering.

From 1985 to 1986 he was an Engineer with the Beijing Institute of Control Engineering, Beijing, China. From 1987 to 1992 he was a Research Assistant at the University of Minnesota, Minneapolis,

MN, and in 1992 he was a part-time software programmer at ProReHab Inc., Roseville, MN, and in 1993 he was a Research Fellow in the Department of Physiology and Biophysics, Mayo Foundation, Rochester, MN. He is currently working at Rosemount Inc., Chanhassen, MN.



James F. Greenleaf (M'73-SM'84-F'88) received the B.S. degree in engineering science in 1968 from Purdue University, West Lafayette, IN, and the Ph.D. degree in engineering science in 1970 from the Mayo Graduate School of Medicine, Rochester, MN and Purdue University.

He is a Professor of biophysics and medicine at the Mayo Medical School and a Consultant at the Biodynamics Research Unit, Department of Physiology, Biophysics, and Cardiovascular Disease and Medicine, Mayo Foundation. His special field

of interest is in ultrasonic biomedical imaging science. he has published more than 150 articles and edited four books.

Dr. Greenleaf has served on the IEEE Technical Committee of the Ultrasonics Symposium since 1985. He served on the IEEE/UFC Subcommittees from the Ultrasonics in Medicine/IEEE Measurement Guide Editors, and on the IEEE Medical Ultrasound Committee. He is the President of the IEEE UFC Society. He holds five patents and is the recipient of the 1986 J. Holmes Pioneer Award from the American Institute of Ultrasound in Medicine. He is a Fellow of the AUIM. He is also the Distinguished Lecturer for the IEEE UFC Society for 1990-1991.